Adjustment of the Southern Ocean to Wind Forcing on Synoptic Time Scales

WILBERT WEIJER AND SARAH T. GILLE

Physical Oceanography Research Division, Scripps Institution of Oceanography, La Jolla, California

(Manuscript received 14 October 2004, in final form 25 April 2005)

ABSTRACT

This study addresses the response of the Southern Ocean to high-frequency wind forcing, focusing on the impact of several barotropic modes on the circumpolar transport. A suite of experiments is performed with an unstratified model of the Southern Ocean, forced with a stochastic wind stress that contains a large range of frequencies with synoptic time scales. The Southern Ocean adjustment displays a different character for frequencies below and above 0.2 cpd. The low-frequency range is dominated by an "almost-free-mode" response in the region where contours of f/H are obstructed by only a few bathymetric features; the truly free mode only plays a minor role. Topographic form stress, rather than friction, is the dominant decay mechanism of the Southern Mode. It leads to a spindown time scale on the order of 3 days. For the high-frequency range, the circumpolar transport is dominated by the resonant excitation of oscillatory modes. The "active" response of the ocean leads to strong changes and even discontinuities in the phase relation between transport and wind stress.

1. Introduction

The Southern Ocean is known for its harsh wind regime, which is the most severe to be found on the earth. Not only are the mean zonal winds among the strongest in the world, but they are also extremely variable; the standard deviation of zonal wind stress variability easily exceeds the mean (Gille 2005). Southern Ocean winds vary over a broad range of frequencies ranging from interannual variability, represented by the Southern Annular Mode (SAM; Thompson and Wallace 2000), up to superinertial fluctuations.

Observational evidence suggests that the response of the Southern Ocean is highly barotropic for subseasonal time scales (e.g., Peterson 1998). The transport variability is hence to a large extent topographically steered (e.g., Gille 1997). In particular, details of the bathymetry and the unique circumpolar configuration of the Southern Ocean seem to give rise to barotropic modes. Several of these modes have been identified in observations and high-resolution general circulation models (GCMs). This investigation uses a simple unstratified process model to probe the details of these modal responses and their impact on the circumpolar transport.

A central role in the ocean response to atmospheric variability seems to be played by a circumpolar Southern Mode in the ocean. For variability on time scales exceeding about 10 days, Hughes et al. (1999, hereinafter HMH) argued for the importance of a free barotropic mode in areas containing contours of f/H that are continuous around Antarctica. Unconstrained by vorticity dynamics, it is expected to respond rapidly and barotropically to changes in the wind forcing. HMH furthermore argued for a so-called almost-free mode: in the area adjacent to the free-mode region where contours of f/H are obstructed by a few topographic features only (like the bathymetry of Drake Passage), only a small and local source of vorticity would be enough to generate a circumpolar response. The geometry of this almost-free-mode region is not well defined, since the ability for the flow to cross contours of f/H depends on the characteristics of the wind stress curl. In this paper, the term Southern Mode will be used to denote both the free and almost-free modes.

If truly free, the Southern Mode would accelerate in response to forcing, resulting in a 90° phase lag. The observed negligible time lag between atmospheric forc-

Corresponding author address: Wilbert Weijer, Physical Oceanography Research Division, Scripps Institution of Oceanography, La Jolla, CA 92093-0230.
E-mail: wweijer@ucsd.edu

ing and ocean response is clearly at odds with this. Analysis of model results made HMH conclude that it "is not the inviscid free mode response that dominates, but either a viscously damped free mode or the almost free mode that requires wind forcing for the current to cross f/H contours in certain locations." Among the aims of this study is to determine the role played by the free and almost-free modes in the Southern Mode response and to identify the process that dampens it.

The Southern Mode is not the only mode that may be excited by wind stress variability; several other types of modal variability have been identified over the years. A category of topographically trapped modes has recently been found in altimeter data (Fu and Smith 1996; Fu 2003) and ocean models (Fukumori et al. 1998; Webb and De Cuevas 2002a,b, 2003). They appear as areas of high variability in specific basins, particularly related to abyssal plains in the southeast Pacific and the southeast Indian Oceans. Although the modes were originally identified as being oscillatory with long periods of about 30 days (Fukumori et al. 1998) and damping time scales exceeding 20 days (Fu 2003), Webb and De Cuevas showed that the modes in the Southern Ocean actually have zero frequency and a damping time scale of only a few days. In this paper, we will refer to these modes as "abyssal-plain modes."

Platzman et al. (1981) calculated the normal modes of a global barotropic ocean for periods between 8 and 80 h and found several modes with expressions in the Southern Ocean. Some of these modes were related to topographic features and could be identified as topographically trapped vorticity waves. Other modes showed characteristics of gravity waves, some with a maximum expression around the Antarctic continent that is characteristic of the fundamental Kelvin wave. A recent investigation of tide gauge data by Ponte and Hirose (2004) has confirmed the presence of Kelvin modes, coastally trapped around the Antarctic continent and excited by atmospheric forcing.

Despite their often local character, many of these modes could influence the circumpolar transport. Indeed, even the most localized modes of Platzman et al. (1981) (i.e., their Kerguelen mode 13) have a clear circumpolar expression as they project on the Antarctic Kelvin modes. This may not be without consequence, since an active, resonant response of the ocean may disrupt a simple, causal relationship, as was illustrated by Weijer (2005). In a simple channel model of the Southern Ocean forced with stochastic winds, the excitation of a normal mode dominated the ocean response to such an extent that the phase relation between the net transport through the channel and the wind stress forcing was inverted by the resonance; for frequencies lower than the resonant frequency (0.3 cpd), the transport seemed to lead the forcing. This raises the question of to what extent normal modes dominate the response when more realistic bathymetry is taken into account. Can we expect a simple relation between transport and wind stress when a suite of resonant modes is excited?

This study uses a constant-density, multilevel model of the Southern Ocean to look at the ocean response to wind forcing over a broad range of frequencies. In particular we investigate the extent to which the barotropic modes play a role in the Southern Ocean response to wind stress variability. We will focus on the frequency range at which they are active and how they affect the phase relation between the circumpolar transport and the wind stress. In addition, we will address the dynamics of the Southern Mode by proposing form stress as the process that is responsible for limiting the growth of the circumpolar flow in response to a variable zonal wind stress. This study aims to describe transport variability on time scales shorter than a few weeks, putting our knowledge about the different modes of adjustment in a single framework.

2. The model

The mean flow of the Antarctic Circumpolar Current (ACC) is usually described as equivalent barotropic (Killworth 1992; Killworth and Hughes 2002). The extent to which this holds for the variability is unclear, but the excitation of a baroclinic response is likely to depend on the spatial and temporal scales of the disturbance in relation to the dominant baroclinic modes. Veronis and Stommel (1956) have shown that motions with spatial scales larger than the Rossby radius of deformation are primarily barotropic, while most of the energy of small-scale motions is baroclinic. This accounts for Killworth's (1992) observation that eddy-kinetic energy in a modeled Southern Ocean displays a self-similar structure in the vertical; with spatial scales of the order of the internal radius of deformation, mesoscale variability is likely to be equivalent-barotropic. In this study we consider perturbations with spatial scales of the order of the external Rossby radius, and periods of the order of weeks; hence we may expect the response to be predominantly barotropic. Indeed, in the channel model of Weijer (2005), the high-frequency response did not depend on the stratification at all, and turned out to be purely barotropic. In addition, the response was not affected by the presence of an ACC or the background circulation in general. Therefore, we will use an ocean model with constant density, starting from the state of rest. Note, however, that small-scale flows induced by bathymetry violate the Rossby radius

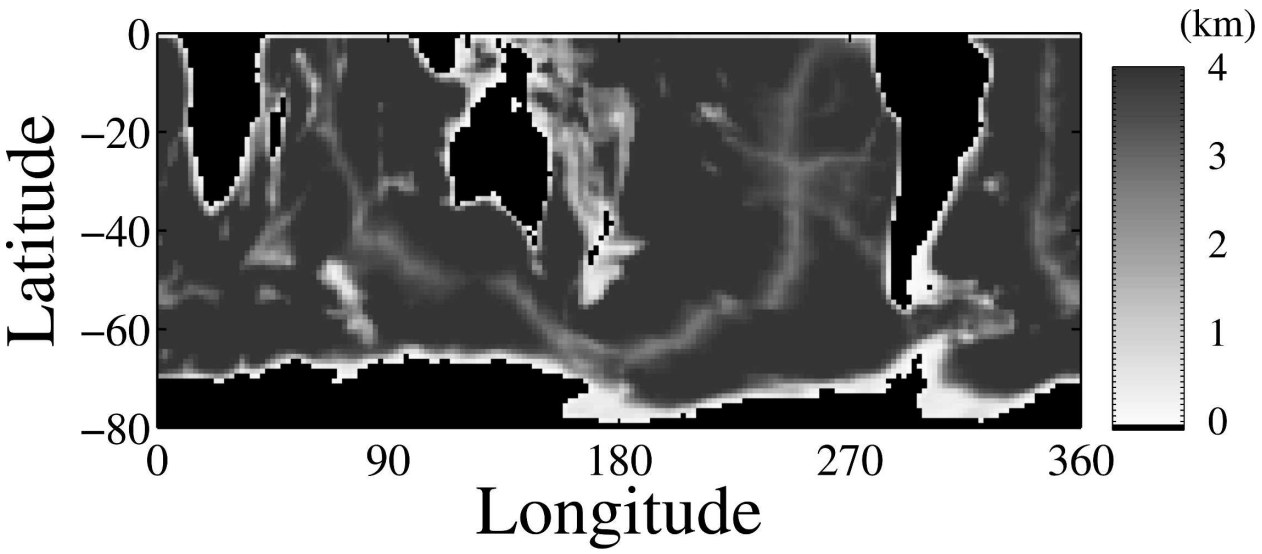

FIG. 1. Bathymetry of the Southern Hemisphere ocean model.

argument and in reality may lead to some baroclinic response. In view of the high frequencies considered here, however, we expect the model response to be qualitatively robust.

A constant-density version of the fully 3D Massachusetts Institute of Technology GCM (MITgcm) is used (Marshall et al. 1997a,b), solving the momentum and continuity equations only. By using a multilayer model, we are able to distinguish between the Ekman transports and geostrophic flows, which are physically separated.

The model domain is taken to be the entire Southern Hemisphere, from 80°S to the equator. Bathymetry is based on the ETOPO-2 dataset (Fig. 1), which is interpolated onto the model grid and smoothed with a Laplace filter. The maximum depth is taken to be 4000 m. A spherical grid is used with 180×80 grid points in the zonal and meridional directions, yielding a horizontal resolution of $2° \times 1°$. The 15 grid points in the vertical direction are unequally distributed, with vertical grid spacing ranging from 62 m for the uppermost layer to almost 600 m for the deepest layer. The model is integrated for 455 days, with a time step $\Delta t = 1200$ s.

Surface pressure is treated by the implicit free-surface formulation, as formulated by Dukowicz and Smith (1994). This approach is known to modify the damping characteristics and wave velocity of gravity and Rossby waves. The essential parameter governing the representation of gravity waves is the Courant–Friedrichs–Lewy number, $k\Delta t c_g$, where k is the wavenumber, Δt is the time step, and c_g is the wave speed. For the large wavelengths associated with the lowest-order Kelvin modes, and the small time step, this number is much smaller than 1. Hence, we do not expect a significant modification of the phase velocity of circumpolar Kelvin modes. In addition, the Kelvin waves have a cross-shore spatial scale on the order of the Rossby radius of deformation, so the waves are well resolved by our numerical grid. Hence, we also do not expect significant modification of the barotropic waves because of insufficient resolution (Hsieh et al. 1983).

Frictional effects are parameterized by ordinary Laplacian friction, with vertical and horizontal viscosity coefficients $A_v = 5.0 \times 10^4$ m^2 s^{-1} and $A_h = 1.0 \times 10^{-3}$ m^2 s^{-1}. No-slip boundary conditions are applied to the lateral boundaries, while a quadratic friction law is applied in the bottom layer, with drag coefficient $C_d = 0.0014$.

Although atmospheric pressure fluctuations may provide an additional forcing mechanism for the ocean on time scales up to 3 days (Ponte 1994), for reasons of simplicity we chose to force the model with wind stress only. A zonal wind stress is applied: $\tau^x(\theta, t_n) = \tau_0 \sigma_n T(\theta)$, where τ_0 is a basic wind stress amplitude (taken to be 0.1 N m^{-2}), and σ_n is a stochastic time series. The spatial profile $T(\theta)$ is zonally constant but has a Gaussian profile in the latitudinal direction, with a maximum at 53°S and a 10° half-width. This profile is chosen to reflect the zonally averaged mean zonal wind stress from climatologies (e.g., Gille 2005). Wearn and Baker (1980, hereinafter WB) and Gille (1999) have shown that transport fluctuations of the ACC are more coherent with zonally averaged wind stress than with local wind stress fluctuations, so this seems a natural initial choice. A study taking into account spatially varying wind fields is currently in progress.

The effect of the belt of strong mean winds is re-

flected in the spatial distribution of the variance of the forcing. This approach accounts for the fact that the variability of the forcing depends on the background state, with stronger variability in the regions where the averaged winds are stronger (e.g., Sura 2003); the strongest variability is hence found at 53°S. Nonetheless, the noise is not truly multiplicative as advocated by Sura (2003) and Sura and Gille (2003), since at a given latitude, the distribution of wind stress is strictly Gaussian.

No background forcing is imposed; on the small time scales considered here the background flow is not expected to affect the barotropic response significantly. The importance of advective terms with respect to the Coriolis term is measured by the Rossby number, $\varepsilon = U_0/fL$. The spatial scales of the disturbances under consideration are on the order of the Rossby radius [$L = O(2 \times 10^6$ m)], so a strong jet with $U_0 = 0.5$ m s^{-1} (Nowlin and Klinck 1986) results in $\varepsilon = O(10^{-3})$. On time scales of roughly $\tau = 5$ days the advective terms are an order of magnitude smaller than the tendency term. Weijer (2005) found that the background flow did not influence the model's barotropic response in a noticeable way.

A stochastic time series σ_n is used as described by Weijer (2005). It is constructed as a summation of N frequency components, equally distributed between $f_{\min}$ and $f_{\max}$. The phases ϕ_i of the frequency components contain a random variable, which allows the time series to continue infinitely without repetition. The amplitudes α_i of the components are inversely proportional to the corresponding frequency through a parameter γ, which determines the spectral slope of the power spectrum. One of the advantages of this method is that it allows for restarting model runs without rendering the stochastic time series discontinuous. Only the phase of each frequency component needs to be known to continue the time series without distorting the spectral characteristics.

In this study, $N = 100$ frequency components are taken. The frequencies range from $f_{\min} = 0.14$ cpd to $f_{\max} = 36$ cpd, corresponding to periods between 7 days and 40 min (the minimum period resolved by the 20-min time step). This corresponds to the high-frequency range considered by Gille (2005). A value of $\gamma = 1.5$ is used throughout this study. Experiments with other spectral slopes indicate that the response of the ocean is linear, and that the transfer function is independent of the specifics of the energy distribution of the forcing (cf. Frankignoul and Müller 1979; Willebrand et al. 1980; Large et al. 1991). The value chosen is in the middle of the range of spectral slopes from different wind products, as determined by Gille (2005) for the Southern Ocean.

TABLE 1. Short summary of model experiments discussed; H_{DP} is the depth of the undersea wall that replaces the Scotia Arc in some experiments. Entry "Gain" shows the gain factor of Drake Passage transport at the lowest resolved frequency (0.018 cpd). This indicates the degree of reddening of the transport spectra.

Run identifier	Characteristic	Gain
R_0	Standard configuration	16.56
R_{RL}	Rigid-lid approximation	18.01
$R_{6\mathrm{km}}$	Max depth is increased from 4 to 6 km	10.25
$R_{1500\mathrm{DP}}$	$H_{\mathrm{DP}} = 1500$ m	7.63
$R_{1000\mathrm{DP}}$	$H_{\mathrm{DP}} = 1000$ m	5.06
$R_{500\mathrm{DP}}$	$H_{\mathrm{DP}} = 500$ m	3.07
$R_{0\mathrm{DP}}$	$H_{\mathrm{DP}} = 0$ m, Drake Passage is closed	—
$R_{2\mathrm{Ah}}$	Doubled horizontal viscosity	16.39
$R_{5\mathrm{Av}}$	Fivefold vertical viscosity	16.56
$R_{2\mathrm{Cd}}$	Doubled drag coefficient	16.56

A series of simulations have been performed, differing mainly in their bathymetry and frictional parameters. Table 1 summarizes these runs.

3. Southern Ocean response to stochastic forcing

a. Sea-surface variability

A first impression of the response of the Southern Ocean to the stochastic forcing is provided by Fig. 2a, which shows the root-mean-square (rms) of the sea level for the standard run ($|\eta| = \sqrt{\langle \eta^2 \rangle}$, where $\langle\rangle$ denotes a time average). Clearly, the largest variability is found south of the latitude where the winds are strongest—that is, south of 53°S—while little variance is found north of it. A simple explanation for this is the fact that a change in circumpolar transport requires a change in the net meridional sea-surface gradient, and hence a meridional redistribution of mass. Since the area to the north of the circumpolar current is substantially larger than the area to the south of it, this exchange causes sea-surface fluctuations to be much stronger in the south than in the north.

The sea-surface variability is hence strongly related to variability of the circumpolar flow. Geostrophic theory predicts an equivalence between sea-surface elevation η and the streamfunction ψ of the depth-integrated flow. Figure 3a displays the rms of the streamfunction field, $|\psi|$; it shows a strong similarity with Fig. 2a.

Although this model has no background mean flow and the time-averaged field of ψ vanishes, the preferred pathway of the oscillating flow is evident from $|\psi|$ as the region with strongest concentration of streamlines. The

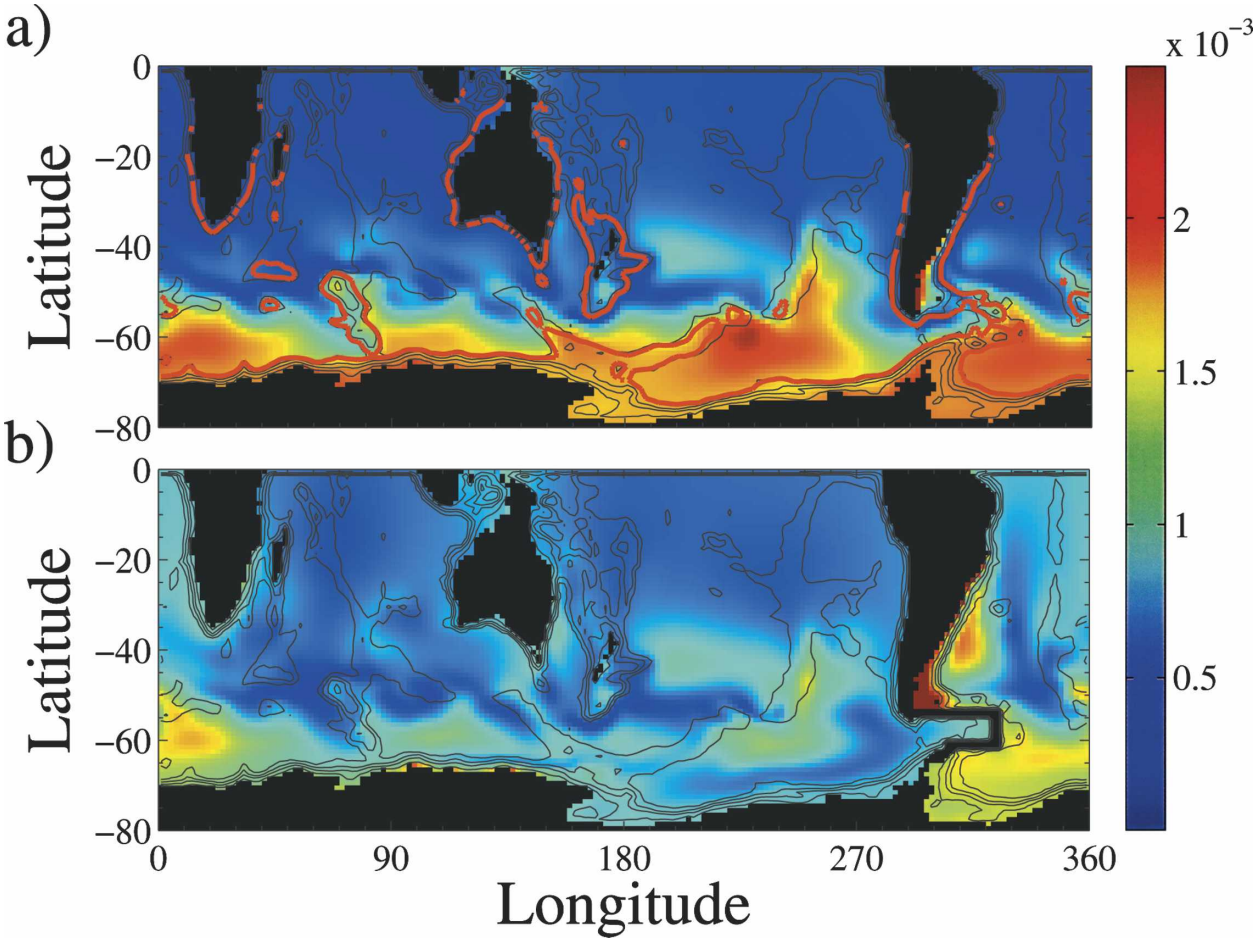

FIG. 2. Rms of sea level η for (a) the standard run R_0 and (b) run R_{0DP} with closed DP. The color scales are the same to facilitate comparison. The red line in (a) denotes the contour $|f/H| = 3.96 \times 10^{-8}$ m s^{-1}, the smallest value that is still continuous around Antarctica. Black lines are isobaths of 500, 1500, 2500, and 3500 m. Note that the oceanic spectra are basically red, so this plot emphasizes patterns of low-frequency variability.

jet is in general zonally oriented, but is clearly deflected by the major bathymetric obstacles. It is situated in HMH's almost-free-mode region, where circumpolar contours of f/H are obstructed by a few major bathymetric features only. The vorticity forcing of our wind stress must be strong, however, since the flow does not follow contours of f/H quite closely.

The red lines in Figs. 2a and 3a denote the contour with the smallest value of $|f/H|$ that is still continuous in our model; it hence bounds the free-mode region as identified by HMH. Although it clearly shows large variability in η and ψ, it contains almost no streamlines, and hence does not carry much volume transport. The free-mode section occupies more than one-third of the width of the Drake Passage at 70°W, but its transport variance is only 0.004 Sv^2 (where 1 Sv $\equiv 10^6$ m^3 s^{-1}) as compared with 0.384 Sv^2 for the entire section.

In addition to the free-mode area, other regions of high variability stand out north of the red contour. Strong maxima are present above the Amundsen Abyssal Plain in the southeast Pacific (60°S, 140°W), the Weddell Abyssal Plain (67°S, 30°W), and the Enderby Abyssal Plain (62°S, 20°E). An additional region of enhanced variability is found in the Australian–Antarctic Basin around 120°E, at 62°S. The localized nature of these regions and their high variance suggests that these modes may be similar to the abyssal-plain modes found in the Southern Ocean by altimetry. In the next section we will show that their spectral characteristics support this interpretation.

b. *Spectra*

The spectral characteristics of the transport variability are presented in Figs. 4 and 5. Figure 4 shows the spectra of the forcing and the transport through Drake Passage for the standard run R_0. However, a clearer

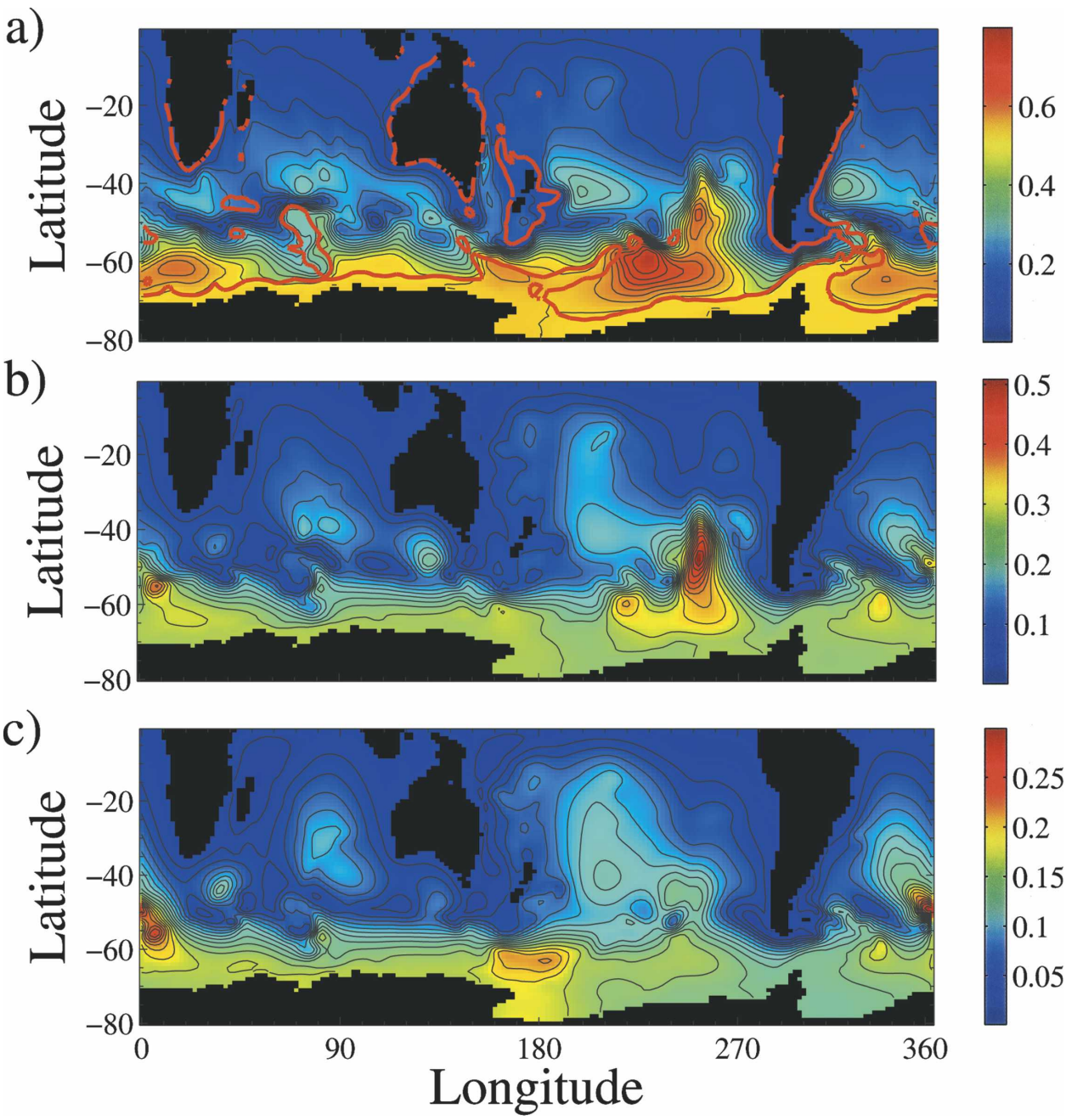

FIG. 3. Rms of (a) the barotropic streamfunction, $|\psi|$, and after applying a (b) 10-day ($|\psi_{10d}|$) and (c) 5-day ($|\psi_{5d}|$) high-pass filter. The area-mean values are subtracted from the daily-averaged fields of ψ. Red line in upper plot is as in Fig. 2.

picture of the response is provided by the gain factor G. This is defined as $\sqrt{P_T/P_\tau}$ where P_τ is the spectrum of the wind stress time series, and P_T is that of Drake Passage transport (Fig. 5, black line).

A prominent aspect of these plots is the reddening of the spectrum; the gain increases with decreasing frequency. Another feature is the presence of peaks of enhanced response in the high-frequency range. These peaks reflect the resonant excitation of several oscillatory modes in the system. In the following sections we will study this signal in more detail and will identify some of the modes that are responsible for this ocean response.

1) THE SOUTHERN MODE

The Southern Mode is essentially a real mode in the sense that it does not possess an inherent oscillatory

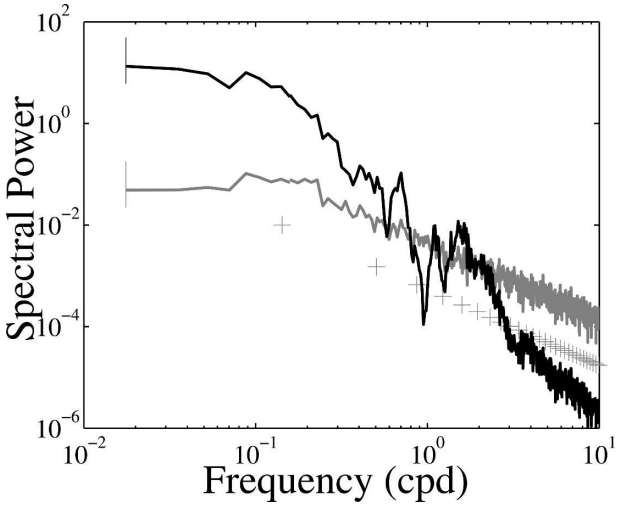

FIG. 4. Spectra of the wind stress forcing (gray line), and of the transport through Drake Passage (black line). Each spectrum is an average over eight members; error bars indicate 95% confidence limits. Pluses denote the (squared) amplitudes of the frequency components that make up the stochastic time series; its spectral slope translates perfectly onto the realized time series. All spectra presented in this paper are a combination of a "normal" spectrum for frequencies lower than 0.1 cpd and a prewhitened spectrum for higher frequencies. Prewhitening was found to be essential for a good representation of the high frequencies, but it tends to corrupt the low frequencies.

time scale. Hence, it can respond to any forcing frequency. The theory of the stochastic excitation of ocean variability predicts its response to increase with decreasing frequency (Hasselmann 1976). The reddening of the spectrum in Fig. 5 (black line) for frequencies below 0.2 cpd is in agreement with these ideas.

Drake Passage with its Scotia Island Arc is the crucial bottleneck for the Southern Mode, since here the bathymetry obstructs most of the f/H contours. To study the impact of sill geometry on the Southern Mode response, three additional runs were performed ($R_{1500\mathrm{DP}}$, $R_{1000\mathrm{DP}}$, and $R_{500\mathrm{DP}}$) in which the Scotia Arc was replaced by an undersea wall of varying depth. Reducing the depth of the Scotia Arc essentially increases the value of $|f/H|$ over the topography. This reduces the range of f/H values that are continuous around Antarctica and squeezes the free-mode region against the Antarctic continent. The impact of reducing the sill depth is immediately clear from Fig. 6: the gain factor is strongly reduced for frequencies below 0.2 cpd. In contrast, the high-frequency modal activity (discussed below) is clearly not hindered by the reduced depth.

An additional calculation was performed in which the maximum depth was increased from 4 to 6 km ($R_{6\mathrm{km}}$). This change does not affect the free-mode region, since its area is shallower than 4000 m everywhere. It does, however, deepen abyssal features in the almost-free-mode region, which were leveled off in the standard calculation. The 15 vertical levels were maintained, but the grid spacing was increased by a factor of 1.5. The piecewise continuous representation of topography in the MITgcm allows deep topographic features to be resolved despite the grid spacing of almost 900 m. Figure 6 shows that the change in maximum depth modifies the low-frequency response in much the same way as changing the Scotia Ridge depth does,

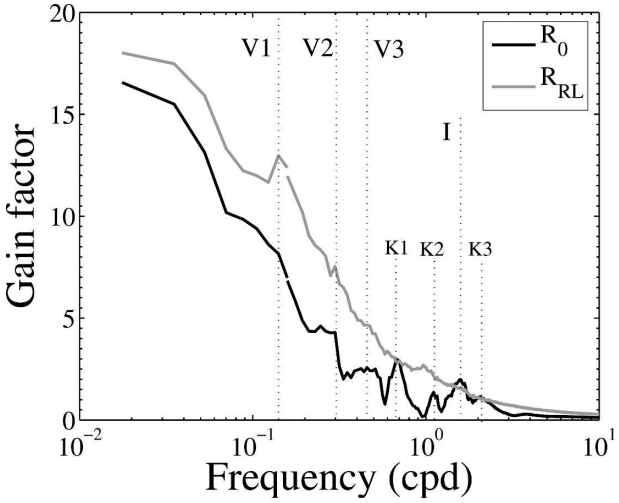

FIG. 5. Gain factor of the transport through Drake Passage. Each spectrum is an average over eight members. Black curve is for the standard run R_0, which has an implicit free-surface formulation for surface pressure; light-gray line is for the rigid-lid simulation R_{RL}. Vertical dotted lines indicate the main oscillatory signals as discussed in the text.

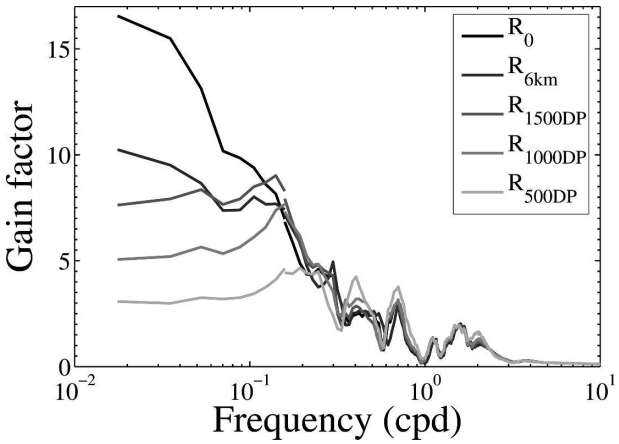

FIG. 6. Gain factor for the standard run R_0, the run with maximum depth of 6 km ($R_{6\mathrm{km}}$), and the runs $R_{1500\mathrm{DP}}$, $R_{1000\mathrm{DP}}$, and $R_{500\mathrm{DP}}$. In the latter, the Scotia Arc is replaced by an undersea wall of 1500-, 1000-, and 500-m depth (see Fig. 2b for the actual geometry of this "Scotia wall").

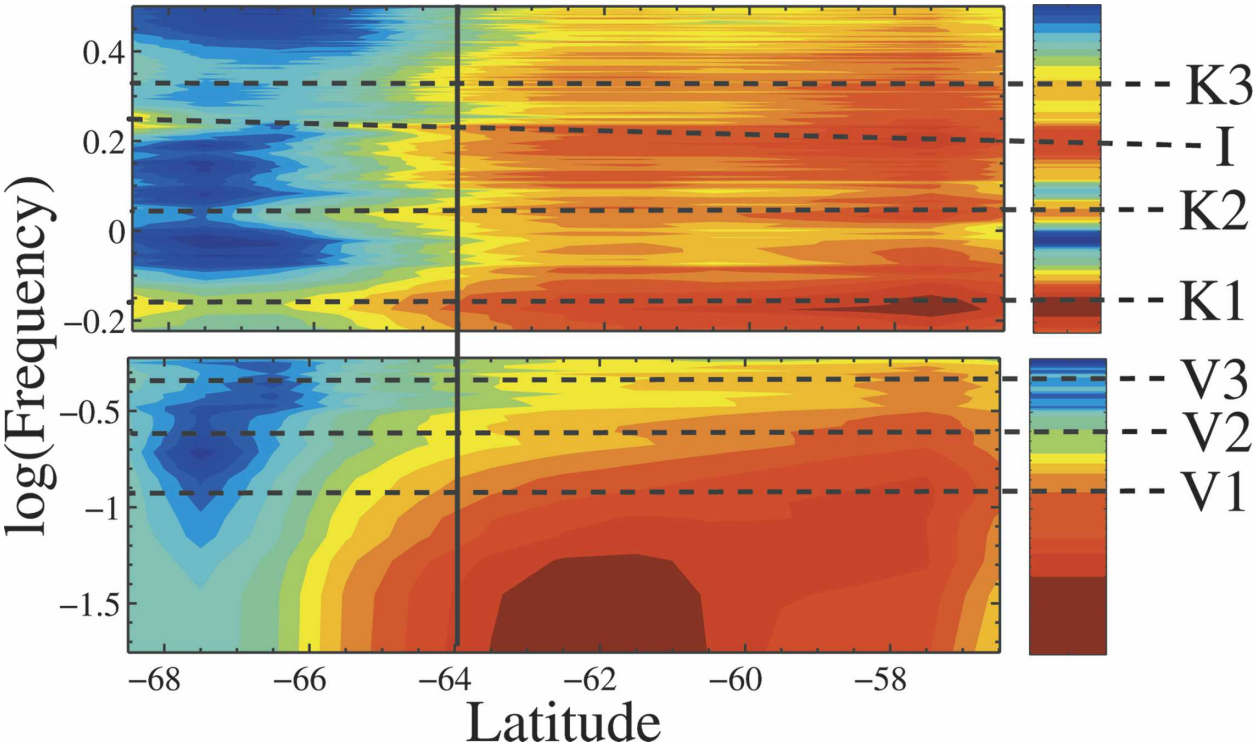

FIG. 7. Base-10 logarithm of the gain factor G of the transport through the Drake Passage, as a function of latitude. Color intervals are (top) 0.13 and (bottom) 0.2. Maximum values (dark red) correspond to $G = 0.4$ and 2.5, respectively. Vertical black line denotes the latitude south of which contours of f/H are zonally continuous. Dashed horizontal lines denote the main oscillatory modes, as in Fig. 5. Boxes on the right denote the gain factor of the total transport.

despite the fact that the bathymetry of the free-mode region itself is not affected. These results confirm the importance of the almost-free mode in determining the transport variability through Drake Passage.

To further assess the importance of the free and almost-free modes, we calculated the spectral characteristics of the circumpolar transport as a function of latitude in the Drake Passage (Fig. 7). The strongest variability takes place in the central and northern part of the Passage, while little variability is found in the free-mode region.

2) THE ABYSSAL-PLAIN MODES

Webb and De Cuevas (2003) showed that the abyssal-plain modes may also be real modes that do not have an oscillatory character. A run with a closed Drake Passage (a Scotia wall of 0-m depth, R_{0DP}) allows us to study the strength and spectral characteristics of these abyssal-plain modes in isolation from the Southern Mode (Fig. 2b).

Figure 8 shows the gain factor of pressure at 58°S, for R_0 and R_{0DP}. For R_{0DP}, the low-frequency variability at 20°E, 120°E, and 140°W can fully be ascribed to the abyssal-plain modes. It is clear that in these regions the modes are associated with an overall reddening of the spectrum for frequencies below 0.1 cpd. In addition, there is no sign of a specific maximum in frequency above 0.02 cpd that could point to the resonant excitation of an oscillatory mode. This supports the findings of Webb and De Cuevas that these modes are real and not oscillatory.

3) HIGH-FREQUENCY MODES

In this section the high-frequency spectral peaks in Fig. 5 will be addressed. Interpreting every peak, however, is beyond the goal of this paper; a study aimed at calculating the normal modes of the Southern Ocean is currently in progress. Nonetheless, some inferences can be made when the standard run is compared with an identical run performed under rigid-lid conditions (Fig. 5, light-gray line). This change filters out most of the modal energy for frequencies exceeding 0.6 cpd. Hence, these peaks most likely represent some form of gravity wave modes.

(i) The inertial mode

The region of enhanced energy around 1.6 cpd (0.6 days, mode "*I*" in Fig. 5) corresponds roughly to the

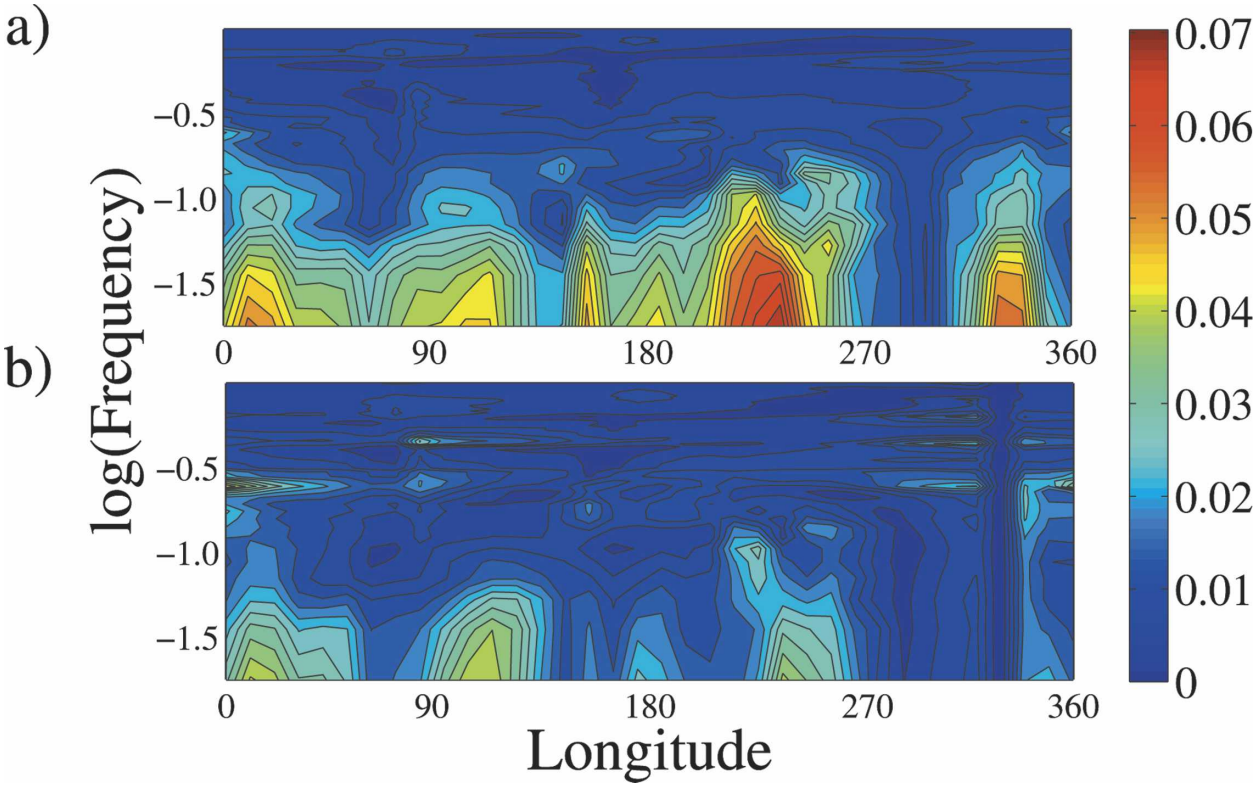

FIG. 8. Gain factor of pressure as function of log(f) and longitude at 58°S for (a) R_0 and (b) R_{0DP} with closed Drake Passage.

inertial band at 53°S, which is the latitude of maximum wind stress amplitude. However, the inertial signal disappears under rigid-lid conditions. In addition, unlike most of the other signals, this peak is unaffected by reducing the depth of the Scotia Ridge. This suggests that the presence of enhanced energy at inertial frequencies in the Drake Passage may actually reflect a Kelvin wave that is excited by the interaction of the inertial oscillations with the South American coast (e.g., Hughes et al. 1999).

(ii) Gravity wave modes

Other spectral peaks are found for frequencies of 0.68 (period of 1.5 days, "K_1"), 1.11 (0.9 days, "K_2") and 2.05 (0.49 days, "K_3"), but a broad dome-shaped maximum centered at 0.46 cpd (2.2 days, "V_3") is also visible in Fig. 5, as is a maximum between 0.26 and 0.30 cpd (3.8 and 3.4 days, "V_2") and a peak at about 0.12 cpd (8.3 days, "V_1").

Peak K_1 at 0.68 cpd probably reflects the fundamental Kelvin mode around the Antarctic continent, as found by Ponte and Hirose (2004) in tide-gauge data, and predicted by the normal-mode analysis of Platzman et al. (1981). Its period is unaffected by the shallowing of the Scotia Sill, but its amplitude is enhanced somewhat for H_{DP} = 500 m. Higher-order Kelvin waves would be expected for frequencies close to 1.36 and 2.04 cpd. The first frequency, if present, would be indiscernible from the broad peak of the inertial band. A peak at 2.05 cpd, however, is visible as K_3 in Fig. 5.

(iii) Topographic modes

The peaks V_1, V_2, and V_3 are likely related to the resonant excitation of topographically trapped modes. The first can be traced back to an energetic region of variability at the East-Pacific Rise. A peak at this frequency is visible at 110°W in both panels of Fig. 8. Figures 3b and 3c show the rms of the 10-day ($|\psi_{10d}|$) and 5-day ($|\psi_{5d}|$) high-pass filtered streamfunction fields, respectively. Mode V_1 is the dominant mode of variability in Fig. 3b. Consistent with its 8.3-day period, it is absent in the 5-day filtered fields.

Similarly, V_2 is related to an energetic oscillatory mode at the Mid-Atlantic Ridge. It is the dominant mode of variability in Fig. 3c, consistent with its 3.5-day period. The dome V_3 centered at 0.46 cpd can be seen to develop into a sharp spectral peak located at 0.40 cpd when the Scotia Sill becomes shallower (Fig. 6). A signal close to this frequency can be seen at several longitudes for the closed Drake Passage run (Fig. 8); its

maximum seems to be related to the Kerguelen ridge at 80°E. Indeed, a localized maximum is visible in the high-pass filtered streamfunctions (Figs. 3b,c).

Although these modes are topographically trapped oscillations, the presence of their signal in the transport spectrum shows that they have a global impact. Modes V_2 and V_3 seem to interact with the Antarctic continent, spawning Kelvin waves that transport their signal around Antarctica (Fig. 8b). The waves generate changes in the meridional pressure gradient, affecting the circumpolar transport. Under rigid-lid conditions, these modes are clearly suppressed (Fig. 5). Mode V_1 may be too far from Antarctica for this mechanism to apply. However, Fig. 3 shows that the resonant mode is in the way of the preferred transport pathway. It hence may affect the circumpolar transport directly.

c. Coherence

Figure 9 shows that there is generally a large coherence between the wind stress time series and the transport through Drake Passage. However, it is reduced or even breaks down at several discrete frequencies that correspond to minima in the gain factor in Fig. 5, and to discontinuities in phase lag (Fig. 9, lower panel). These discontinuities bridge gaps of 30°, 80°, 270°, and 70° for the events at 0.33, 0.58, 1.0, and 1.23 cpd. These phase jumps accommodate the strong phase shifts that are induced by the resonant modes, centered at frequencies of 0.46, 0.68, 1.11, and 1.6 (see Fig. 5).

d. Time scales of the response

The phase lag ϕ of Fig. 9 can simply be translated into a time lag between the transport response and the wind forcing through

$$\tau_1 = -\frac{\phi(f)}{2\pi f}, \tag{1}$$

where ϕ is taken in radians.

Wearn and Baker (1980) proposed a very simple model to relate the transport through Drake Passage (Ψ) to the zonally averaged wind stress (T):

$$\frac{d\Psi}{dt} = T - r\Psi. \tag{2}$$

Here, $1/r$ is a frictional time scale, which they estimated to be on the order of 9 days. Since the system is linear (see Fig. 5), Eq. (2) should hold for every frequency component individually, so that in Fourier space we have

$$[2\pi i f + r(f)]\Psi^*(f) = T^*(f), \tag{3}$$

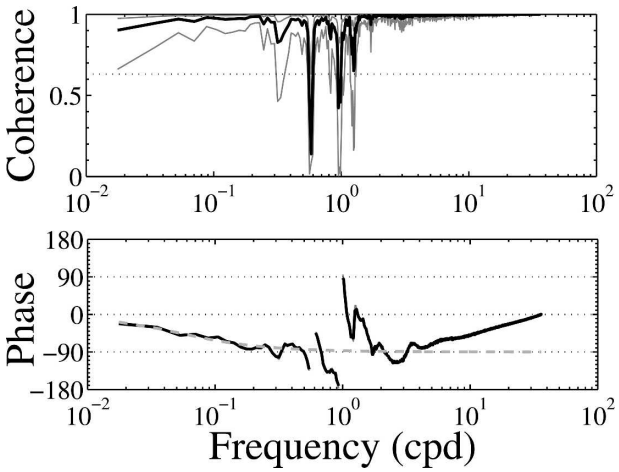

FIG. 9. (top) Coherence and (bottom) phase between the wind stress time series and the transport through Drake Passage. The spectra are averaged over eight members. Dotted line in upper panel gives 95% significance level based on a zero-coherence test; light-gray lines denote 95% confidence limits (Von Storch and Zwiers 1999, p. 285). Only phases are plotted that correspond to coherences significantly differing from zero. Negative phase means that wind leads the transport. 95% confidence limits are plotted according to Von Storch and Zwiers (1999), but are indiscernible from main curve. Gray dashed line in the lower plot shows phase predicted by the model of WB for a frictional period of 3 days.

where we allow r to depend on frequency. If we take T^* to be real-valued, we can determine the real and imaginary parts of Ψ^* and relate r to the phase angle ϕ. The resulting frictional time scale is then

$$\tau_2 = \frac{1}{r} = \frac{\tan\phi}{2\pi f}. \tag{4}$$

Figure 10 shows the actual time lag τ_1 and the frictional time scale τ_2. Both time scales decay rapidly for the highest frequencies, and attain values of approximately 3 days for the lowest frequencies. For frequencies higher than 0.2 cpd, the time scales show complex behavior, and they are negative in certain regions in frequency space. In this region, the model response is strongly influenced by the resonant modes, and Eq. (2) essentially breaks down. The time scales compare well for small phase angles ϕ, but τ_1 is generally smaller than τ_2. This is in agreement with the results of WB, and also follows from a small-angle expansion of τ_2 [Eq. (4)].

The gray dashed line in the lower panel of Fig. 9 shows the phase predicted by the WB model for a frictional time scale τ_2 of 3 days. Its correspondence with the actual phase for frequencies below 0.2 cpd is striking. This suggests that the simple model captures the basic physics of the low-frequency barotropic response of the ACC in Drake Passage.

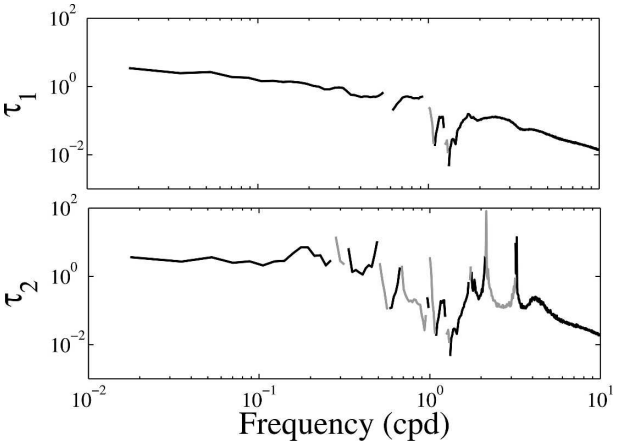

FIG. 10. Time scales of ocean response for the run with $\gamma = 1.5$. (top) The actual lag τ_1 between transport and forcing [according to Eq. (1)]. (bottom) The frictional time scale τ_2 as deduced from the model of WB [according to Eq. (4)]. Gray sections of the curves denote negative lag (transport leads forcing).

e. Form stress

The question remains as to what mechanism sets the decay time scale. To test the sensitivity of these results to frictional parameterizations of the model, we conducted similar experiments for doubled horizontal viscosity ($A_h = 1 \times 10^5$ m^2 s^{-1}), a fivefold increase in vertical viscosity ($A_v = 5 \times 10^{-3}$ m^2 s^{-1}), and a doubled bottom friction coefficient ($C_d = 0.0028$). None of these changes produced an ocean response different from the basic run (see the "Gain" entry in Table 1). Also the time scales of the response are basically unaffected.

The most obvious alternative for the decay is the form stress. Let us consider the zonal momentum balance, distinguishing between the Ekman flow, which is forced directly by the wind stress, and the barotropic interior. For the time scales longer than 5 days (for which WB's model was shown to hold) a purely meridional Ekman transport M^y is in balance with a zonal wind stress: $M^y = -\tau^x/\rho_0 f$. Let us furthermore assume the interior flow (u_g, v_g) to be linear and frictionless. The change in zonal momentum of the interior flow, integrated over depth h and along latitude lines, satisfies

$$\rho_0 \frac{\partial}{\partial t} \oint u_g h \, dx = f\rho_0 \oint v_g h \, dx - g\rho_0 \oint h\eta_x \, dx$$

$$= \oint \tau^x \, dx - g\rho_0 \oint h\eta_x \, dx. \qquad (5)$$

Here, the net meridional transport in the interior is supposed to balance the Ekman transport. Comparisons of this with Eq. (2) indicate that the form stress must provide the deceleration, schematically represented by $-r\Psi$ in Eq. (2). The form stress term is hard to evaluate analytically, but Fig. 11 shows that the relation between the transport through Drake Passage and the stress term, integrated over the area south of 56°S, is linear.

But is its magnitude large enough? Suppose that form stress F acts to remove the total circumpolar zonal momentum P according to $dP/dt = -F$. This expression can be cast in terms of Ψ and compared with Eq. (2) to obtain r. First, F is expressed in terms of Ψ by formalizing their linear relation through $F = \zeta\Psi$, where ζ is the slope of 0.056 TN Sv^{-1} (Fig. 11). Then the total zonal circumpolar momentum P is defined as the integral of ρu over the entire circumpolar volume. If we assume the transport (velocity times cross-sectional area) to be zonally coherent, we can estimate: $P = \rho_0 \Psi L$, where $L = 20 \times 10^6$ m measures the zonal extent of the Southern Ocean at Drake Passage latitudes. This yields $d\Psi/dt = -r\Psi$, with $r^{-1} = \rho_0 L/\zeta$, which is equivalent to a decay time scale of about 4 days. This shows that the form stress is strong enough to provide the brake on the ACC that ultimately balances the wind stress forcing.

4. Summary and discussion

In this paper we have studied the response of the Southern Ocean to high-frequency variability in wind stress forcing. In particular we have focused on the role of barotropic modes in this adjustment. The ocean response displayed a clear dichotomy for frequencies above and below 0.2 cpd. For the high-frequency range, the resonant excitation of oscillatory modes dominated the adjustment of the circumpolar transport to wind

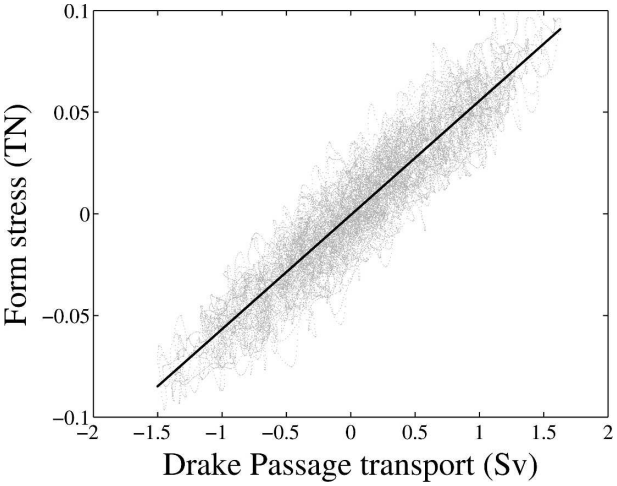

FIG. 11. Relation between barotropic transport through Drake Passage (Sv) and the form stress (10^{12} N), which is the last term in Eq. (5), integrated over the area south of 56°S.

stress variability, while the Southern Mode generated a red response at lower frequencies.

a. Low-frequency response: $f < 0.2$ cpd

The results presented in this paper support the notion that low-frequency transport variability is dominated by an almost-free mode in the Southern Ocean, as suggested by HMH. The region where an almost-free mode can exist is not well defined, and it depends to some extent on the characteristics of the wind stress. In this model, the preferred path of circumpolar transport was found north of 60°S. It crossed many contours of f/H on its path deflected by bathymetric obstacles.

In contrast, in this model the truly free mode plays a negligible role, accounting for less than 10% of the transport variability through the Drake Passage. High variability in sea-surface height in this region can be seen as a passive response to transport variability farther north. There is no indication of "autonomous" variability in this region (except for coastally trapped waves).

The transport through Drake Passage is highly coherent with the wind stress, which is not surprising in a model where the forcing is the only source of variability. However, neither the phase lag nor the time lag was found to be constant. The 3-day lag is small enough, though, to be consistent with recent results suggesting a "negligible" time lag (Hughes et al. 1999; Aoki 2002). For frequencies lower than 0.2 cpd, this time lag was well captured by the simple model of WB, who modeled the Southern Ocean response to wind stress as a simple balance between acceleration of the zonal flow, input of zonal momentum by the wind, and a linear decay term.

The success of the WB model requires a strong decay term with a spindown time scale of only 3 days. However, the model response turned out to be insensitive to the value of frictional parameters of the model. This suggests that this spindown does not reflect the action of frictional processes. The only candidate that could provide a force strong enough to explain the short frictional time scale is the form stress. Indeed, a rough estimate of this term yields a damping time scale of the right order of magnitude.

Form stress has been recognized as the principal mechanism balancing the momentum input by the zonal mean winds in the Southern Ocean (Munk and Palmén 1951). Krupitsky and Cane (1994) and Wang and Huang (1995) corroborated the balance between topographic form drag and wind stress for the steady barotropic circulation in their circumpolar channel models. Their analyses focused on supercritical topography in which all contours of f/H are blocked. The strong decay in this model supports the conclusion that the transport is not dominated by an inviscid free mode, since form stress cannot act on free flow following contours of f/H.

These results suggest that the representation of barotropic variability in numerical models benefits from an accurate bathymetry, and is rather insensitive to the frictional closures. The first conclusion is in line with Hirose et al. (2001), who studied barotropic variability in a shallow-water model, but the second is not. In a shallow-water model, the Ekman transports are spread out over the entire water column, rather than being confined in a surface layer. It may be that the resulting strong abyssal flows overemphasize the importance of friction.

In addition to the Southern Mode, topographically trapped modes were excited, which showed up as localized areas of high variability in the Southern Ocean (specifically related to the Weddell, Enderby, and Amundsen Abyssal Plains at 30°W, 20°E and 140°W, and the Australian–Antarctic Basin at 120°E, in Fig. 2). Similar modes have recently been found in altimeter data (Fu and Smith 1996; Fu 2003) and in ocean models (Fukumori et al. 1998; Webb and De Cuevas 2002a,b, 2003), although their positions disagree slightly. The observations (Fu and Smith 1996) show the southeast Pacific mode at a more easterly position above the Bellinghausen, rather than the Amundsen Abyssal Plain. Similarly, a maximum in the Enderby sector seems positioned at 50°E, to the east of our maximum. The Weddell mode lies mainly out of reach of the Ocean Topography Experiment (TOPEX)/Poseidon and hence may have escaped detection; the model study by Fukumori et al. (1998, their plate 2a) does show a clear maximum there. The strong mode in the Australian–Antarctic Basin is relatively weak in our model. It seems unlikely that the spatial resolution, or the interpolation and smoothing of the bathymetry are responsible for these discrepancies. Indeed, $R_{6\text{km}}$ and the standard run repeated with double horizontal resolution displayed basically the same pattern of variability (not shown). The discrepancies must be ascribed to our choice for a fixed pattern of wind stress, which may be suboptimal for the excitation of some of the modes. Centering the band of wind stress at 48°S does strike an energetic mode in the Australian–Antarctic Basin. Similarly, our wind stress may be more optimal to excite the Weddell and Enderby modes than in reality.

The pressure variations in the centers of these modes show essentially red spectra down to at least frequencies of 0.02 cpd. This supports the findings of Webb and De Cuevas that these modes may be real, rather than complex, and hence have zero frequency. This aspect

makes them hard to distinguish from the Southern Mode based on time series alone. It is therefore impossible to tell whether these modes, which are essentially geographically localized, have an impact on the circumpolar transport. At 58°S latitude, each of these modes seems to be geographically localized, but they form the boundary of the preferred path of the circumpolar transport. A comparison of the panels in Figs. 2 and 8 shows that the variance of the abyssal-plain modes decreases when Drake Passage is closed. It is, however, not clear whether the almost free component of the Southern Mode is superimposed on the abyssal-plain modes so that its absence reveals their true strengths, or whether the modes somehow interact. The former possibility seems most likely considering the linear character of our model.

b. High-frequency response: $f > 0.2$ cpd

For periods shorter than 5 days, the ocean response is dominated by the resonant excitation of oscillatory modes. These modes are related to inertial motions, Kelvin modes, and topographic modes. They show up as peaks in the transport spectra (Fig. 5). Ponte and Hirose (2004) found Kelvin waves in tide gauge observations, and they have shown that Kelvin modes may be excited by fluctuations in surface pressure. The results presented here show that they may also respond to wind stress.

The presence of these oscillatory modes has important implications for the coherence between the transport and the wind stress: at the resonant frequencies strong changes in the phases were observed, accompanied by discontinuities in the phases at the frequencies in between. In some geophysical systems, the excitation of resonant modes is known to lead to interesting phase behavior. Webb (1973) has shown an example of "negative age" of tides in the Coral Sea, where spring tides precede the full or new moon by a day or so. Necessary ingredients for this behavior are a resonance in the system and some kind of decay process. In Weijer (2005), a channel model of the Southern Ocean displayed a complete phase reversal between the transport and wind stress, as a result of a resonant mode. However, if multiple resonant modes are excited, the importance of each of them is reduced, leading to more moderate and less permanent phase changes. Most studies estimating the coherence only fully resolved periods exceeding about a week (e.g., Gille et al. 2001); the results presented here show that the behavior on shorter periods is likely to be governed by different physical processes.

Meredith and Hughes (2004) recently compared bottom pressure measurements from Kerguelen and Amsterdam Islands with the SAM index. They found little coherence of the SAM index with the Amsterdam record but significant coherence with the Kerguelen record for time scales exceeding 50 days. The latter did not display an inverse relation (high winds, low pressure), as would be expected for a region influenced by the Southern Mode, but a positive correlation. In addition, a phase discontinuity seemed to be present at 0.023 cpd, with pressure leading the wind stress for lower frequencies. This resembles the behavior induced by resonant oscillatory modes seen in Fig. 9 and in Weijer (2005).

In our model, a topographic resonance is present as mode V_3, which may be related to Kerguelen mode 13 of Platzman et al. (1981). However, the time scale of this mode is too small to explain the observations of Meredith and Hughes (2004). In addition, pressure at the Kerguelen site does display the inverse phase relationship with wind stress that is characteristic of a site under influence of the Southern Mode (not shown). It would be interesting to see if the results of Meredith and Hughes (2004) indeed reflect a low-frequency resonant mode around the Kerguelen Plateau, and whether its absence in our model points at too low resolution to resolve the relevant bathymetry, or at a mode of baroclinic variability.

5. Conclusions

This study has provided a unifying picture of modes of Southern Ocean variability that are active on time scales from a day to several weeks. This seems especially worthwhile in view of the link between the SAM and the circumpolar transport that has recently been found (Aoki 2002; Hall and Visbeck 2002; Hughes et al. 2003; Meredith et al. 2004). The dominance of the Southern Mode in controlling circumpolar transport for time scales exceeding a week is convenient because of its relatively simple dynamics. It leads to a rather straightforward relation between transport and wind stress. Its independence of frictional closure seems good news from a modeling point of view, since models seem to suffer from a certain arbitrariness in their closure schemes. Instead, it puts the burden on a correct representation of the bathymetry.

The high-frequency range, on the other hand, is dominated by a series of oscillatory modes that inhibit a consistent forcing-transport relationship. Only a systematic identification of the excitable modes will enable us to fully explain the ocean response in this regime.

Acknowledgments. This research was supported by the NASA Ocean Vector Wind Science Team, JPL Contract 1222984. Constructive reviews from Mike Meredith (British Antarctic Survey) and an anonymous reviewer are gratefully acknowledged.

REFERENCES

Aoki, S., 2002: Coherent sea level response to the Antarctic Oscillation. *Geophys. Res. Lett.,* **29,** 1950, doi:10.1029/2002GL015733.

Dukowicz, J. K., and R. D. Smith, 1994: Implicit free-surface method for the Bryan-Cox-Semtner ocean model. *J. Geophys. Res.,* **99,** 7991–8014.

Frankignoul, C., and P. Müller, 1979: Quasi-geostrophic response of an infinite β-plane ocean to stochastic forcing by the atmosphere. *J. Phys. Oceanogr.,* **9,** 104–127.

Fu, L.-L., 2003: Wind-forced intraseasonal sea level variability of the extratropical oceans. *J. Phys. Oceanogr.,* **33,** 436–449.

——, and R. D. Smith, 1996: Global ocean circulation from satellite altimetry and high-resolution computer simulation. *Bull. Amer. Meteor. Soc.,* **77,** 2625–2636.

Fukumori, I., R. Raghunath, and L.-L. Fu, 1998: Nature of global large-scale sea level variability in relation to atmospheric forcing: A modeling study. *J. Geophys. Res.,* **103,** 5493–5512.

Gille, S. T., 1997: The Southern Ocean momentum balance: Evidence for topographic effects from numerical model output and altimeter data. *J. Phys. Oceanogr.,* **27,** 2219–2232.

——, 1999: Evaluating Southern Ocean response to wind forcing. *Phys. Chem. Earth,* **24A,** 423–428.

——, 2005: Statistical characterization of zonal and meridional ocean wind stress. *J. Atmos. Oceanic Technol.,* **22,** 1353–1372.

——, D. P. Stevens, R. T. Tokmakian, and K. J. Heywood, 2001: Antarctic Circumpolar Current response to zonally averaged winds. *J. Geophys. Res.,* **106,** 2743–2759.

Hall, A., and M. Visbeck, 2002: Synchronous variability in the Southern Hemisphere atmosphere, sea ice, and ocean resulting from the Annular Mode. *J. Climate,* **15,** 3043–3057.

Hasselmann, K., 1976: Stochastic climate models. Part I: Theory. *Tellus,* **28,** 473–485.

Hirose, N., I. Fukumori, and V. Zlotnicki, 2001: Modeling the high-frequency barotropic response of the ocean to atmospheric disturbances: Sensitivity to forcing, topography, and friction. *J. Geophys. Res.,* **106,** 30 987–30 995.

Hsieh, W., M. K. Davey, and R. C. Wajsowicz, 1983: The free Kelvin wave in finite-difference numerical models. *J. Phys. Oceanogr.,* **13,** 1383–1397.

Hughes, C. W., M. P. Meredith, and K. J. Heywood, 1999: Wind-driven transport fluctuations through Drake Passage: A Southern Mode. *J. Phys. Oceanogr.,* **29,** 1971–1992.

——, P. L. Woodworth, M. P. Meredith, V. Stepanov, T. Whitworth, and A. R. Pyne, 2003: Coherence of Antarctic sea levels, Southern Hemisphere Annular Mode, and flow through Drake Passage. *Geophys. Res. Lett.,* **30,** 1464, doi:10.1029/2003GL017240.

Killworth, P. D., 1992: An equivalent-barotropic mode in the Fine Resolution Antarctic Model. *J. Phys. Oceanogr.,* **22,** 1379–1387.

——, and C. W. Hughes, 2002: The Antarctic Circumpolar Current as a free equivalent barotropic jet. *J. Mar. Res.,* **60,** 19–45.

Krupitsky, A., and M. A. Cane, 1994: On topographic pressure drag in a zonal channel. *J. Mar. Res.,* **52,** 1–23.

Large, W. G., W. R. Holland, and J. C. Evans, 1991: Quasi-geostrophic ocean response to real wind forcing: The effects of temporal smoothing. *J. Phys. Oceanogr.,* **21,** 998–1017.

Marshall, J., A. Adcroft, C. Hill, L. Perelman, and C. Heisey, 1997a: A finite-volume, incompressible Navier-Stokes model for studies of the ocean on parallel computers. *J. Geophys. Res.,* **102,** 5753–5766.

——, C. Hill, L. Perelman, and A. Adcroft, 1997b: Hydrostatic, quasi-hydrostatic, and non-hydrostatic ocean modeling. *J. Geophys. Res.,* **102,** 5733–5752.

Meredith, M. P., and C. W. Hughes, 2004: On the wind forcing of bottom pressure variability at Amsterdam and Kerguelen Islands, southern Indian Ocean. *J. Geophys. Res.,* **109,** C03012, doi:10.1029/2003JC002060.

——, P. L. Woodworth, C. W. Hughes, and V. Stepanov, 2004: Changes in the ocean transport through the Drake Passage during the 1980s and 1990s, forced by changes in the Southern Annular Mode. *Geophys. Res. Lett.,* **31,** L21305, doi:10.1029/2004GL021169.

Munk, W. H., and E. Palmén, 1951: Note on the dynamics of the Antarctic Circumpolar Current. *Tellus,* **3,** 53–55.

Nowlin, W. D., and J. M. Klinck, 1986: The physics of the Antarctic Circumpolar Current. *Rev. Geophys.,* **24,** 469–491.

Peterson, R. G., 1998: On the transport of the Antarctic Circumpolar Current through Drake Passage and its relation to wind. *J. Geophys. Res.,* **93,** 13 993–14 004.

Platzman, G. W., G. A. Curtis, K. S. Hansen, and R. D. Slater, 1981: Normal modes of the World Ocean. Part II: Description of modes in the period range 8 to 80 hours. *J. Phys. Oceanogr.,* **11,** 579–603.

Ponte, R. M., 1994: Understanding the relation between wind- and pressure-driven sea level variability. *J. Geophys. Res.,* **99,** 8033–8039.

——, and N. Hirose, 2004: Propagating bottom pressure signals around Antarctica at 1–2-day periods and implications for ocean modes. *J. Phys. Oceanogr.,* **34,** 284–292.

Sura, P., 2003: Stochastic analysis of Southern and Pacific Ocean sea surface winds. *J. Atmos. Sci.,* **60,** 654–666.

——, and S. T. Gille, 2003: Interpreting wind-driven Southern Ocean variability in a stochastic framework. *J. Mar. Res.,* **61,** 313–334.

Thompson, D. W. J., and J. M. Wallace, 2000: Annular modes in the extratropical circulation. Part I: Month-to-month variability. *J. Climate,* **13,** 1000–1016.

Veronis, G., and H. Stommel, 1956: The action of variable wind stresses on a stratified ocean. *J. Mar. Res.,* **15,** 43–75.

Von Storch, H., and F. W. Zwiers, 1999: *Statistical Analysis in Climate Research.* Cambridge University Press, 484 pp.

Wang, L., and R. X. Huang, 1995: A linear homogeneous model of wind-driven circulation in a β-plane channel. *J. Phys. Oceanogr.,* **25,** 587–603.

Wearn, R. B., and D. J. Baker, 1980: Bottom pressure measurements across the Antarctic Circumpolar Current and their relation to the wind. *Deep-Sea Res.,* **27A,** 875–888.

Webb, D. J., 1973: Tidal resonance in the Coral Sea. *Nature,* **243,** 511.

——, and B. A. De Cuevas, 2002a: An ocean resonance in the Indian sector of the Southern Ocean. *Geophys. Res. Lett.,* **29,** 1664, doi:10.1029/2002GL015270.

——, and ——, 2002b: An ocean resonance in the Southeast Pacific. *Geophys. Res. Lett.,* **29,** 1252, doi:10.1029/2001GL014259.

——, and ——, 2003: The region of large sea surface height variability in the southeast Pacific Ocean. *J. Phys. Oceanogr.,* **33,** 1044–1056.

Weijer, W., 2005: High-frequency wind forcing of a channel model of the ACC: Normal mode excitation. *Ocean Modell.,* **9,** 31–50.

Willebrand, J., S. G. H. Philander, and R. C. Pacanowski, 1980: The oceanic response to large-scale atmospheric disturbances. *J. Phys. Oceanogr.,* **10,** 411–429.